MAGNETIC RESONANCE IN CHEMISTRY
Magn. Reson. Chem. 2006; **44**: 823–831
Published online 6 June 2006 in Wiley InterScience (www.interscience.wiley.com). DOI: 10.1002/mrc.1841

Solid-state NMR characterization of ^{69}Ga and ^{71}Ga in crystalline solids

Jason T. Ash and Philip J. Grandinetti*

Department of Chemistry, The Ohio State University, 120 W. 18th Avenue, Columbus, Ohio 43210-1173, USA

Received 18 December 2005; Revised 23 February 2006; Accepted 24 March 2006

Gallium model systems containing four- and six-coordinate gallium sites have been investigated using solid-state NMR. Measurement of the isotropic chemical shift and electric field gradient (EFG) have been performed at 9.4 T on α-Ga_2O_3, β-Ga_2O_3, $LiGaO_2$, $NaGaO_2$, $KGaO_2$, $Ga_2(SO_4)_3$, and $LaGaO_3$ using a variety of techniques on both NMR active nuclei (^{69}Ga and ^{71}Ga) including static, high speed magic-angle spinning (MAS), satellite transition (ST) spectroscopy, and rotor-assisted population transfer (RAPT). The chemical shift is found to correlate well with the coordination number, with four-coordinate gallium having values of approximately 50 ppm and six-coordinate gallium having values near 225 ppm (referenced to 1 M gallium nitrate solution). The magnitude of the EFG is found to be correlated to the distortion of the gallium polyhedra, with the strained systems having EFGs of 3×10^{21} Vm^{-2} or more, while the less strained systems have values of 1.5×10^{21} Vm^{-2} or less. A plot of chemical shift versus EFG suggests that solid-state NMR of gallium oxyanions can be more discriminating than liquid state NMR chemical shifts alone. Copyright © 2006 John Wiley & Sons, Ltd.

KEYWORDS: gallium NMR; quadrupolar nuclei

INTRODUCTION

Gallium compounds are used in semiconductor devices, superionic conductors,[1,2] laser diodes, zeolites,[3,4] and in medicine for fighting malignancies.[5–7] Despite such wide-ranging applications, the use of gallium NMR in the solid state remains largely undeveloped in comparison with other Group IIIA nuclei such as boron and aluminum. Although ^{71}Ga (40% abundance) has a gyromagnetic ratio and quadrupole moment similar to ^{27}Al ($I = 5/2$), its quadrupolar splittings are typically 3 times larger when experiencing the same EFG simply because it has a lower spin angular momentum of $I = 3/2$. The other NMR active gallium nucleus, ^{69}Ga (60% abundance), also $I = 3/2$, has the additional difficulty that its nuclear quadrupole moment is approximately 60% larger than ^{71}Ga. Overall, these factors lead to such large quadrupolar broadenings (first- and second-order) that NMR resolution and sensitivity of sites in gallium compounds are significantly worse than in boron and aluminum analogs.

Fortunately, a combination of methodological advances in solid-state NMR, such as high speed magic-angle spinning (>30 kHz), variable offset cumulative spectroscopy (VOCS),[8] satellite transition (ST) spectroscopy,[9] rotor-assisted population transfer (RAPT),[10–12] and Multiple-Quantum MAS (MQ MAS),[13–15] have dramatically improved the potential of gallium solid-state NMR. This study was undertaken to improve our understanding of the relationships between structure in gallium compounds and NMR parameters. Model systems such as β-Ga_2O_3, a compound which has been studied extensively by Massiot and coworkers[8,16,17] is examined, as well as α-Ga_2O_3, and other modified gallium oxide systems: $LiGaO_2$, $NaGaO_2$, $KGaO_2$, $Ga_2(SO_4)_3$, and $LaGaO_3$. These systems were chosen because their crystal structures are established in the literature and represent a variety of structural units that are present in numerous materials.

*Correspondence to: Philip J. Grandinetti, Department of Chemistry, The Ohio State University, 120 W. 18th Avenue, Columbus, Ohio 43210-1173, USA. E-mail: grandinetti.1@osu.edu

EXPERIMENTAL

Synthesis

Gallium oxide, lanthanum (III) oxide, gallium (III) chloride, sodium carbonate, lithium carbonate, potassium carbonate, and gallium sulfate were purchased from Alfa Aesar and used as starting materials without further purification. β-Ga_2O_3 was synthesized by heating the oxide at 600 °C for several hours, as this is the stable high temperature polymorph. To synthesize α-Ga_2O_3, gallium (III) chloride was slowly dissolved in water. Gallium oxide hydrate was then precipitated by making the solution basic, using ammonia. In order to ensure crystallinity, the precipitate was subsequently washed repeatedly with hot water over the course of several days before being dehydrated at 400 °C.[18,19] Lithium gallate ($LiGaO_2$), sodium gallate ($NaGaO_2$), and potassium gallate ($KGaO_2$) were synthesized from solid-state reaction by heating stoichiometric mixtures of gallium oxide and the appropriate carbonate at 900 °C. Lanthanum gallate was synthesized by first heating lanthanum (III) oxide

to 1500 °C prior to weighing. Then equimolar amounts of lanthanum (III) oxide and gallium oxide were mixed and fired to 1100 °C.[20,21] Gallium sulfate was heated to 100 °C to ensure dehydration prior to study.

NMR spectroscopy

^{71}Ga and ^{69}Ga static experiments were performed at 122 MHz and 96 MHz respectively, on a Chemagnetics CMX II spectrometer operating at 9.4 T. Unless otherwise stated, all experiments were performed using a Hahn echo sequence with a whole echo acquisition.[22] Magic-angle spinning (MAS) experiments were performed on a Bruker DSX-400 spectrometer also operating at 9.4 T. All MAS experiments were performed using a 2.5 mm rotor spinning at 30 kHz. All spectra were referenced to a 1 M aqueous solution of gallium nitrate. All spectra were processed using the RMN software,[23] and analyzed using the NMR Utilities Software.[24] Effects from other interactions such as chemical shift anisotropy (CSA) and dipole–dipole couplings were neglected in the simulations, as the lineshapes could be reproduced by considering only the isotropic chemical shift and the quadrupole interaction. The large quadrupole coupling constants associated with pure gallium oxides result in spectral widths that span hundreds of kilohertz, making it difficult to uniformly excite the entire static spectrum efficiently at a single carrier frequency. As a result, the spectra of these materials were acquired using the VOCS technique of Massiot and coworkers.[8] In VOCS, the offset of the carrier frequency is varied to excite different regions of the spectrum, and the powder pattern is obtained by summation of the individual spectra. Shown in Fig. 1 is the static ^{69}Ga spectrum of β-Ga_2O_3 obtained using the VOCS technique. Each spectrum was acquired at a different carrier frequency, with the offset being varied by 100 kHz between cross sections. The resulting VOCS spectrum is the sum, shown at the top. Though each offset excites only a portion of the spectrum, it is possible to obtain a uniformly excited spectrum using the VOCS technique.

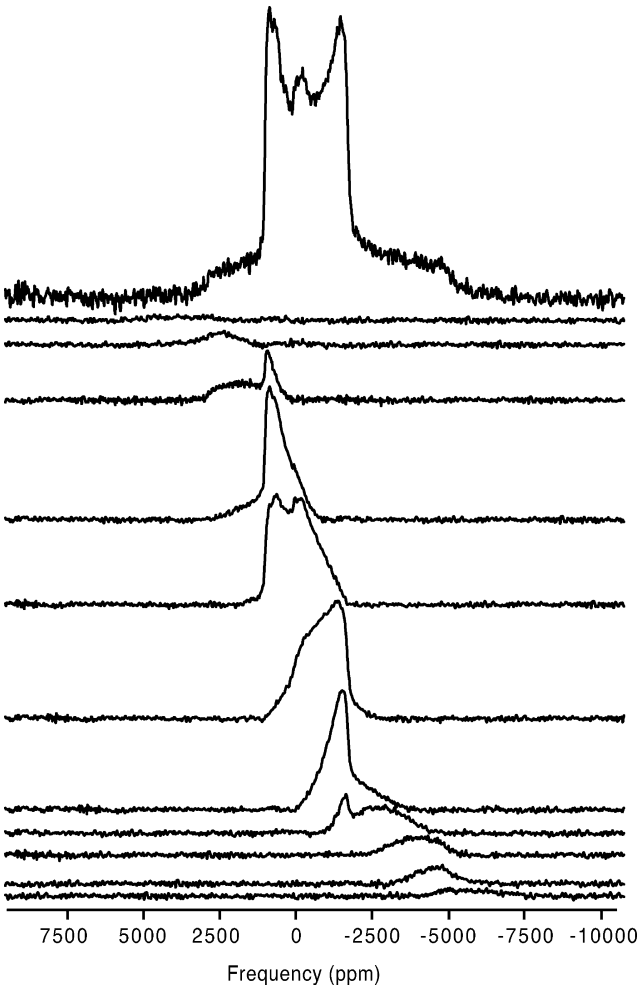

Figure 1. Static ^{69}Ga NMR spectrum of β-Ga_2O_3, acquired using the VOCS technique as described by Massiot and coworkers.[8] For each spectrum, the offset is incremented by 100 kHz, and the full spectrum is obtained by summing the spectra.

RESULTS

General remarks

An advantage of observing two NMR active nuclei is that each site can be parameterized in both spectra with a single EFG and chemical shift tensor. Thus, one obtains the same type of corroborative information about the tensors that can be found by performing experiments at two static fields. The chemical shift for a given site should be the same in both the ^{69}Ga and ^{71}Ga spectra. Additionally, the asymmetry parameter (η), defined in terms of the principle components of the EFG (q) is given by:

$$\eta = \frac{q_{xx} - q_{yy}}{q_{zz}} \tag{1}$$

and should also remain unchanged in both ^{69}Ga and ^{71}Ga. However, the other directly measured quantity is the quadrupole coupling constant C_q, which is given by

$$C_q = \frac{(eQ)(eq_{zz})}{h} \tag{2}$$

and should therefore scale with the electric quadrupole moment (Q) of the nucleus being observed. For gallium, ^{69}Ga has $Q = 1.68\,10^{-29}$ m^2, and ^{71}Ga has $Q = 1.06\ 10^{-29}$ m^2.[25] As a practical note, since the second-order quadrupole broadening is proportional to $q_{zz}{}^2/\nu_0$ (where ν_0 is the Larmor frequency), ^{71}Ga has linewidths more than 3 times narrower than ^{69}Ga, leading to greater signal-to-noise ratio despite the fact that ^{69}Ga is more abundant (60% vs 40%). Finally, it should be noted that, for ease of comparison, a list of relevant structural parameters for all the materials studied is presented in Table 1.

Gallium oxides

The crystal structure of β-Ga_2O_3 has been well established in the literature. It belongs to the monoclinic spacegroup $C2/m$.[27,28] There are two crystallographically inequivalent gallium sites of equal population. One site is coordinated with six oxygen atoms (octahedron) and the other is coordinated with four oxygen atoms (tetrahedron). The tetrahedra are strictly corner sharing, sharing corners with other tetrahedra in the direction of the b-axis and with the octahedra in the other directions, with each corner of the

Table 1. Structural parameters of the model compounds studied, including both average values and standard deviations of the Ga–O bond distances and the O–Ga–O bond angles

Structure	Spacegroup	Site	d_{Ga-O}	$\sigma_{d_{Ga-O}}$	∠Ga–O–Ga	$\sigma_{\angle Ga-O-Ga}$	Reference
α-Ga_2O_3	$R3\bar{c}$	GaO_6	2.00 Å	0.09 Å	89°	9°	26
β-Ga_2O_3	$C2/m$	GaO_6	1.99 Å	0.06 Å	90°	7°	27,28
β-Ga_2O_3	$C2/m$	GaO_4	1.84 Å	0.02 Å	109°	5°	27,28
$LiGaO_2$	$Pna21$	GaO_4^-	1.85 Å	0.01 Å	109°	2°	29
$NaGaO_2$	$Pna21$	GaO_4^-	1.838 Å	0.007 Å	109°	3°	30
$KGaO_2$	$Pbca$	GaO_4^-	1.838 Å	0.006 Å	109°	3°	30
$KGaO_2$	$Pbca$	GaO_4^-	1.837 Å	0.008 Å	109°	3°	30
$Ga_2(SO_4)_3$	$R\bar{3}$	GaO_6^{3-}	1.935 Å	0.006 Å	90°	6°	31
$Ga_2(SO_4)_3$	$R\bar{3}$	GaO_6^{3-}	1.943 Å	0.004 Å	90.0°	0.6°	31
$LaGaO_3$	$Pbnm$	GaO_6^{3-}	1.977 Å	0.003 Å	90°	1°	20

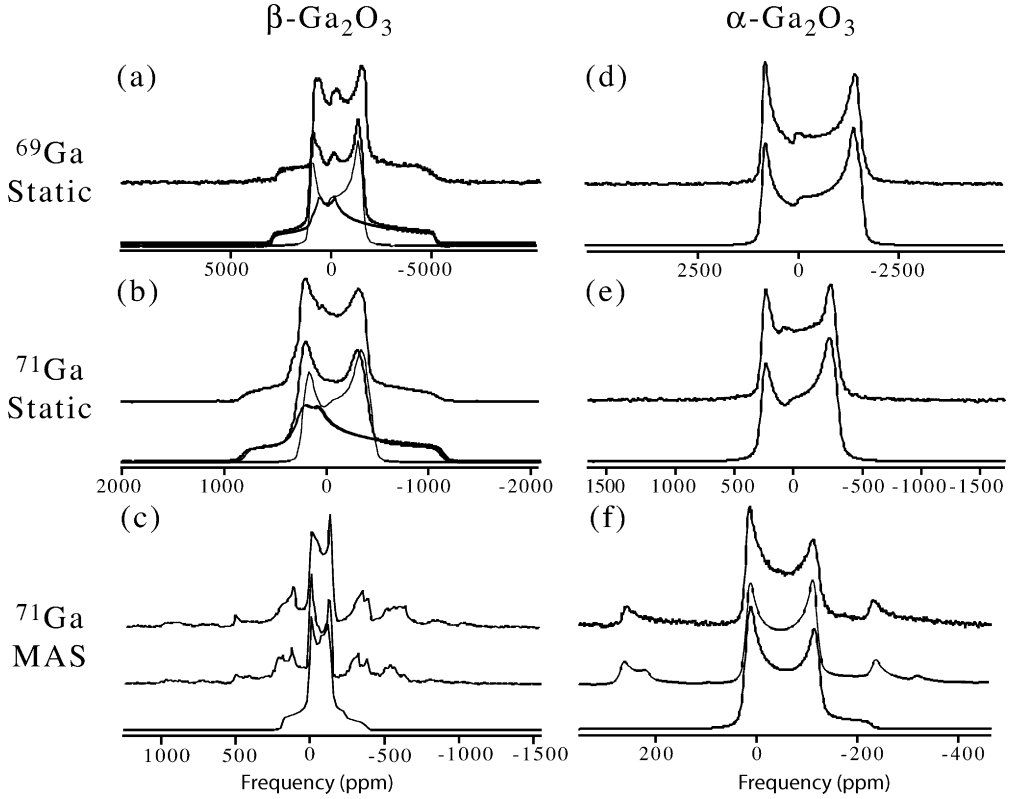

Figure 2. NMR spectra of gallium oxides. In (a), (b), and (c) are the ^{69}Ga static, ^{71}Ga static, and ^{71}Ga MAS spectra of β-Ga_2O_3, respectively. In (d), (e), and (f) are the ^{69}Ga static, ^{71}Ga static, and ^{71}Ga MAS spectra of α-Ga_2O_3, respectively. In (a), (b), (d), and (e), the experimental spectrum is on top, with the simulation below. In (c) and (f), the experimental spectrum is on top, a numerical simulation with 30 kHz spinning speed is in the middle, and an infinite spinning speed simulation below.

tetrahedron being shared among 3–4 polyhedra. Meanwhile, the octahedra also share edges with one another. The structure is largely ionic, as each oxygen atom is coordinated to 3–4 gallium atoms and the polyhedra carry essentially no net electrostatic charge. Hence, to describe these units, the octahedron is denoted as GaO_6 and the tetrahedron is denoted as GaO_4.

In contrast, the metastable α-Ga_2O_3 contains only one gallium site. It belongs to the spacegroup $R3\bar{c}$.[26] Again, the structure is largely ionic. The oxygen atoms are approximately hexagonal and close-packed and all of the gallium atoms are coordinated to six oxygen atoms (GaO_6). Each octahedron shares one of its faces with another octahedron as well as sharing three of its oblique edges with three other octahedra.

Seen in Fig. 2 are the NMR spectra of α- and β-gallium oxide. The static spectra of β-Ga_2O_3 have been studied previously by Massiot and coworkers.[8,16,17] As predicted from the crystal structure, the spectra are described by two equally intense powder patterns. The β-gallium oxide spectrum was assigned by Massiot and coworkers based on the assertion that the GaO_4 site is more distorted from the ideal structure than is the GaO_6 site, and as a result must have a larger C_q. However, the EFG can be highly sensitive to even relatively small differences in bond angles and bond distances, making it difficult to assign the spectrum

based solely on the crystal structure. In this case, the initial assignment can be confirmed by the close agreement between the parameters of α-Ga_2O_3 and the GaO_6 resonance of β-Ga_2O_3. As can be seen in Fig. 2(c), the magnitude of the quadrupole broadening for the GaO_4 site is such that, even under very fast MAS, the experimental spectrum (top) still breaks up into a number of spinning sidebands at this field, making the fitting of the data using standard infinite spinning speed assumptions invalid (bottom). A numerical simulation taking into account the finite spinning speed (middle) does accurately reproduce the spectrum, but it is difficult to estimate uncertainties using such techniques. This is problematic because ^{71}Ga MAS produces lines that are narrower than the others, and is therefore the most accurate determination of the chemical shift. Note that the GaO_6 resonance, as can be seen in Fig. 2(f), can be simulated using standard curve fitting techniques, and the small spinning sidebands can also be reproduced using numerical techniques (Table 2 for the NMR parameters).

Alkali metal gallates

The structures of lithium[29] and sodium gallate[30] both belong to the spacegroup Pna21, while potassium gallate belongs to the spacegroup *Pbca*.[30] Both the lithium and sodium gallate contain a single gallium site, while the potassium gallate possesses two inequivalent sites of equal population. The structures are similar to β-Ga_2O_3 in that the gallium atoms are coordinated by four oxygen atoms. However, unlike β-Ga_2O_3, the tetrahedra share corners with only one other tetrahedron, indicative of a covalent network. The resulting GaO_4 polyhedra now possess a net negative charge (GaO_4^-) which is charge balanced by the cations occupying the gaps between the tetrahedra.

The NMR spectra of the gallates are shown in Fig. 3. Note the much narrower spectral window used in these experiments. There is no longer any need for VOCS, as the entire powder pattern is now uniformly excited with a single carrier frequency. The magnitude of the EFG has been reduced by a factor of 3 relative to the tetrahedra in β-Ga_2O_3, leading to nearly an order of magnitude reduction in linewidth. This reduction in linewidth makes ^{69}Ga MAS possible, which was not feasible in the case of the oxides. This is particularly advantageous in the case of narrower lines, as effects from other interactions such as CSA (and possibly dipole–dipole interactions) may begin to significantly contribute to the lineshape. These interactions are averaged to zero under MAS, whereas the quadrupole coupling is simply scaled, making the MAS powder pattern dependent upon the isotropic chemical shift and the EFG. The precision of the measurement of C_q is determined by the width of the powder pattern, so the broader ^{69}Ga MAS spectrum allows for a more accurate determination of the EFG than does the ^{71}Ga MAS. It should also be noted that while lithium and sodium gallate appear to be stable, potassium gallate was found to be extremely hygroscopic. The sample was found to degrade over the course of several hours under MAS, despite using dried air for all spinning experiments. The NMR parameters determined from the simulations are given in Table 2.

Other structures

Lanthanum Gallate ($LaGaO_3$)

Lanthanum gallate belongs to the orthorhombic spacegroup *Pbnm*.[20] The structure consists of a single gallium site. The oxygen atoms form a slightly distorted and tilted octahedron around the gallium atom. In $LaGaO_3$, the octahedra share corners with one other octahedron, leading to an oxygen coordination number of two. The lanthanum atoms occupy the gaps between the octahedra, coordinating to several oxygen atoms over a much longer distance than the gallium. Thus, lanthanum gallate can be described as GaO_6^{3-}.

This structure has been studied previously.[32] The NMR spectra of lanthanum gallate (GaO_6^{3-}) in Fig. 4 are nearly 25 times narrower than those in α-Ga_2O_3 (GaO_6). The static spectra in Fig. 4(a) and (c) indicate a broadened resonance, but no discernible powder pattern can be simulated. Under MAS, there still exists some suggestion of a powder pattern, but the lack of sharp singularities makes the determination of EFG parameters ambiguous. To ensure that quadrupole coupling was the source of the observed broadening, the ^{71}Ga ST spinning sidebands were excited using a 4 mm rotor spinning at 15 kHz along with a short (0.25 μs) high-power pulse ($\nu_1 = 100$ kHz). The experimental results can be seen in Fig. 4(e) (top). The numerical simulation (bottom) is based on the parameters extracted from the MAS spectrum. While the simulation does not take into account finite pulse effects

Table 2. ^{69}Ga and ^{71}Ga NMR parameters determined in this study with the estimated uncertainty listed in parentheses

Structure	Site	eq_{zz} (10^{21} Vm^{-2})	η	Chemical shift (ppm)	C_q (^{69}Ga) (MHz)	C_q (^{71}Ga) (MHz)
α-Ga_2O_3	GaO_6	3.19 (0.04)	0.08 (0.04)	56 (7)	13.0 (0.2)	8.2 (0.1)
β-Ga_2O_3	GaO_6	3.20 (0.04)	0.12 (0.08)	50 (10)	13.0 (0.2)	8.2 (0.1)
β-Ga_2O_3	GaO_4	4.3 (0.2)	0.90 (0.1)	200 (50)	17.4 (0.8)	11.0 (0.5)
$LiGaO_2$	GaO_4^-	1.52 (0.02)	0.37 (0.02)	242 (2)	6.17 (0.08)	3.89 (0.05)
$NaGaO_2$	GaO_4^-	1.44 (0.02)	0.40 (0.02)	238 (2)	5.84 (0.08)	3.69 (0.05)
$KGaO_2$	GaO_4^-	1.37 (0.08)	0.4 (0.2)	225 (4)	5.6 (0.4)	3.5 (0.3)
$KGaO_2$	GaO_4^-	1.39 (0.08)	0.6 (0.2)	232 (4)	5.64 (0.4)	3.6 (0.3)
$LaGaO_3$	GaO_6^{3-}	0.49 (0.04)	0.5 (0.3)	51 (0.2)	2.0 (0.1)	1.26 (0.09)
$Ga_2(SO_4)_3$	GaO_6^{3-}	0 (n/d)	n/d	−87 (0.1)	0 (n/d)	0 (n/d)
$Ga_2(SO_4)_3$	GaO_6^{3-}	0.73 (0.05)	0.2 (0.2)	−98 (1)	2.9 (0.2)	1.9 (0.1)

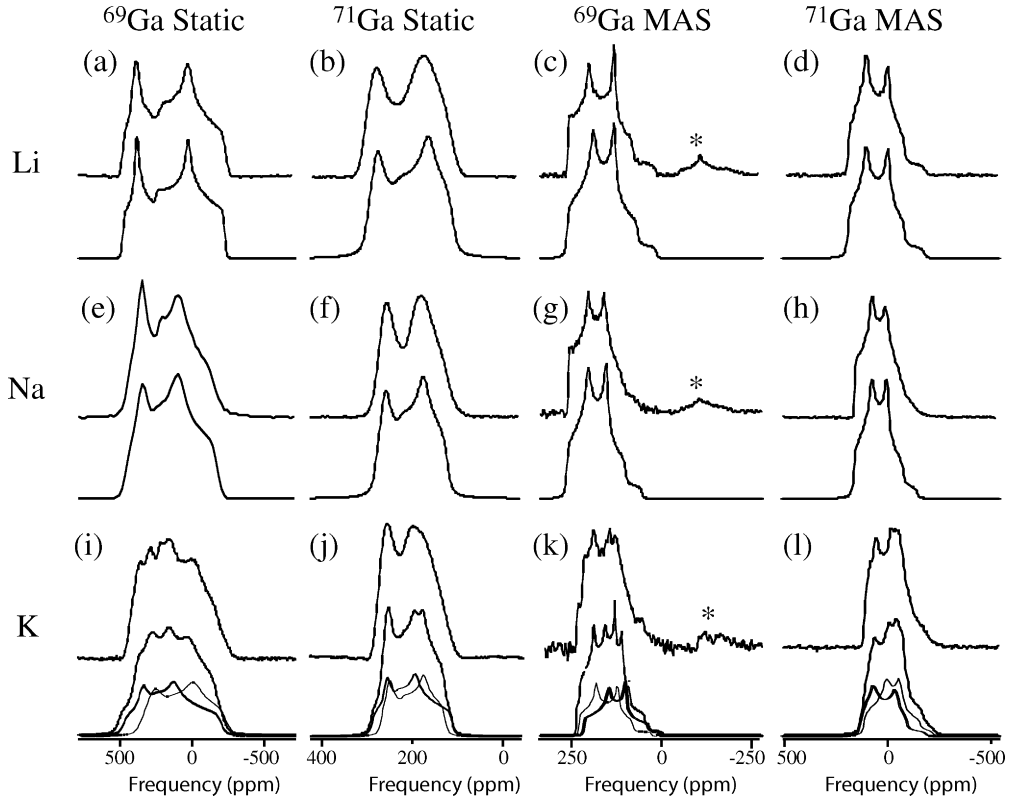

Figure 3. Gallium NMR spectra of the alkali metal gallates. In (a–l), the experimental spectrum is located on top, with the simulation below. In (a–d) are the ^{69}Ga static, ^{71}Ga static, ^{69}Ga MAS, and ^{71}Ga MAS spectra of $LiGaO_2$, respectively. In (e–h) are the ^{69}Ga static, ^{71}Ga static, ^{69}Ga MAS, and ^{71}Ga MAS spectra of $NaGaO_2$, respectively. In (i–l) are the ^{69}Ga static, ^{71}Ga static, ^{69}Ga MAS, and ^{71}Ga MAS spectra of $KGaO_2$, respectively. Asterisks (*) denote the location of spinning sidebands.

or slight magic-angle mis-settings, the span of the spinning sidebands is consistent with the EFG parameters. Similar behavior is observed for ^{69}Ga, but is complicated due to multiple radio-frequency interferences in the 96 ± 2 MHz frequency range.

The assignment of C_q from the simulations can be further confirmed by consideration of the first moment ($\bar{\delta}$) of the two MAS spectra, which is given by:

$$\bar{\delta} = \int \delta f(\delta) \mathrm{d}\delta \tag{3}$$

where the function $f(\delta)$ is the spectrum normalized to have an integral of unity. Unlike the broad powder patterns previously mentioned, $\bar{\delta}$ can be calculated with high precision for $LaGaO_3$. For $I = 3/2$, the first moment of a quadrupole powder pattern under MAS is given by:

$$\bar{\delta} = \delta_{CS}^{iso} + 3\delta_{Q}^{iso} \tag{4}$$

where the two terms on the right hand side represent the isotropic chemical shift and isotropic quadrupole shift, respectively. For $I = 3/2$, the isotropic quadrupole shift is given by:

$$\delta_{Q}^{iso} = -\frac{P_q^2}{120\,\nu_0^2} 10^6;\ P_q = C_q\sqrt{1+\frac{\eta^2}{3}} \tag{5}$$

Since the parameters for ^{69}Ga and ^{71}Ga are related, the two MAS spectra can be used to extract the values of δ_{CS}^{iso} and P_q.

A second independent measurement of C_q can be performed using the RAPT experiment.[10–12] In RAPT, off-resonance Gaussian pulses are used to saturate the STs in order to enhance the central transition. Under static conditions, the STs are broadened by first-order quadrupole interactions and the width of pattern is $\pm\nu_q$ from the central transition, where

$$\nu_q = \frac{3C_q}{2I(2I-1)} \tag{6}$$

For $I = 3/2$, $\nu_q = 0.5C_q$. Thus, if one performs a series of experiments at various offset frequencies, one observes enhancement of the central transition when the offset is within ν_q and the enhancement returns to unity once the offset exceeds ν_q. This series of experiments is termed a *RAPT profile* and the largest offset for which the enhancement is greater than unity is termed the ν_{edge}. Shown in Fig. 5 is the RAPT profile for both ^{71}Ga and ^{69}Ga. Since the ν_{edge} is proportional to C_q, and not P_q, it is possible to use the RAPT profile along with the first moment analysis to extract C_q and η without the use of the central transition lineshape. For ^{69}Ga and ^{71}Ga, the parameters as calculated from a first moment analysis are given in Table 3.

Gallium Sulfate ($Ga_2(SO_4)_3$)

Gallium sulfate belongs to the spacegroup $R\bar{3}$.[31] Like α-Ga_2O_3, the gallium atoms are coordinated by six oxygen atoms, while the sulfur atoms are coordinated by four oxygen atoms. The oxygen atoms of the octahedra share

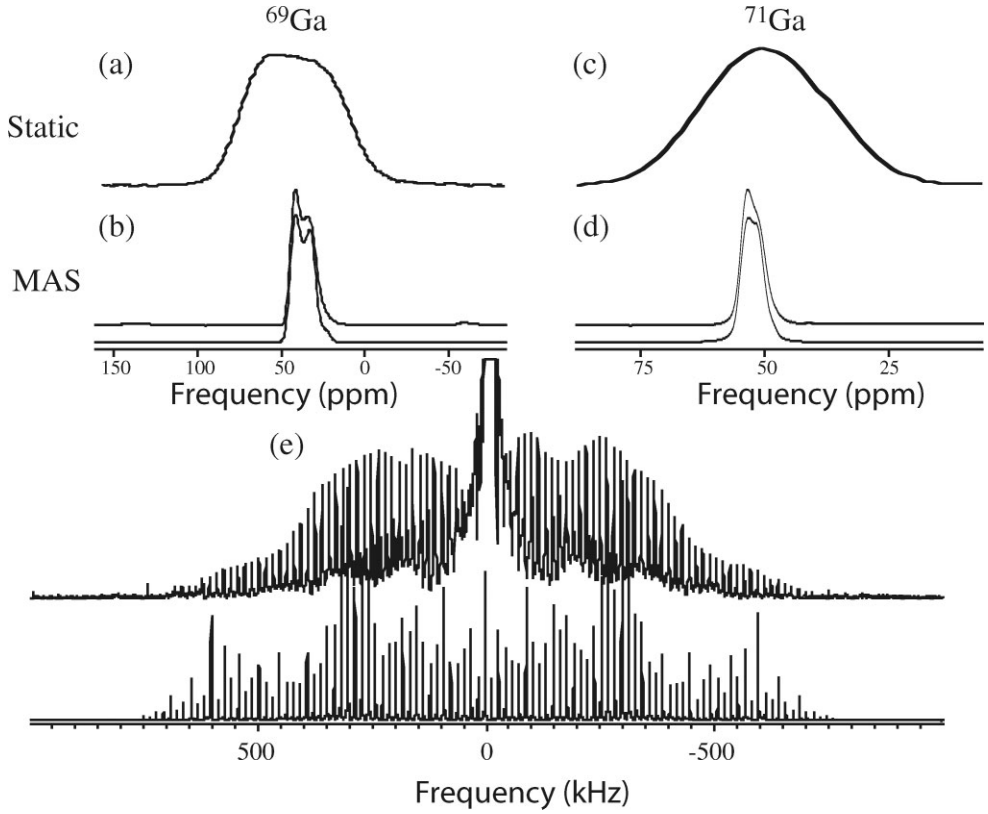

Figure 4. Gallium NMR spectra of $LaGaO_3$. In (a) and (c) are the ^{69}Ga and ^{71}Ga static spectrum. There is no discernible lineshape information in the static spectra. In (b) and (d) are the ^{69}Ga MAS, and ^{71}Ga MAS spectra (top), along with the simulations (below). In (e) is the ^{71}Ga ST spectrum (top), with a numerical simulation of only the STs (below). The central transition, located near 0 kHz, has been truncated to emphasize the STs, and the simulation is based upon the best fit parameters and does not include effects from finite pulses or magic-angle mis-settings.

Table 3. NMR parameters for $LaGaO_3$ as calculated from the first moment of the MAS spectra and the RAPT profile, with uncertainties in parentheses

	^{69}Ga	^{71}Ga
$\bar{\delta}$ (ppm)	43.6 (0.6)	53.0 (0.2)
ν_{edge} (kHz)	1020 (80)	650 (50)
δ_{CS}^{iso} (ppm)	56.1 (0.4)	56.1 (0.4)
P_q (MHz)	2.14 (0.08)	1.35 (0.05)
C_q (MHz)	2.05 (0.08)	1.30 (0.05)
η	0.5 (0.3)	0.5 (0.3)

each corner with a single sulfate tetrahedron, and there is no sharing found among the octahedra (or the tetrahedra for that matter). Thus, each oxygen atom in the structure is coordinated to one gallium atom and one sulfur atom, and the local gallium structure can be described as GaO_6^{3-}. The asymmetric unit consists of two inequivalent GaO_6^{3-} polyhedra, with the principal distinction being a nearly order of magnitude decrease in the deviation of the average O–Ga–O bond angle (Table 1).

The NMR spectra for gallium sulfate is located in Fig. 6. From the static NMR data, evidence for the two inequivalent sites is present. Under MAS conditions, resolution of the inequivalent sites is achieved. In both the ^{69}Ga and ^{71}Ga MAS spectra, one of the sites is sharp and shows no discernible powder pattern. This suggests that the value is too small to be measured. Such an assumption is validated by two observations. First, the nutation rate of the narrow resonance is the same as the rf field, whereas the nutation rates for the other resonances observed thus far have been twice the rf field. Perturbation theory indicates that in the small C_q limit, the site will nutate at $|\gamma B_1|$. But in the large C_q limit, resonances will nutate $I + 1/2$ times faster. Second, unlike the case of $LaGaO_3$, it was not possible to generate any ST spinning sidebands from the narrow resonance, indicating that the C_q must be lower than the spinning speed employed (15 kHz).

Because of this narrow resonance, acquiring a whole echo in the time domain is difficult, as this resonance dephases much slower than the quadrupole powder patterns. In addition, obtaining a spectrum that was totally quantitative was not possible. Instead, for the high speed MAS, a shifted echo was employed with the delay between the two pulses corresponding to three rotor periods (100 μs). The data was then shifted postacquisition to ensure that the point at $t = 0$ corresponded to the maximum of the echo. This has the advantages of delaying the initial acquisition to avoid probe ringdown problems, while avoiding sensitivity losses and lineshape distortions associated with the long echo delay that would be required to record a whole echo spectrum. The NMR parameters can be seen in Table 2.

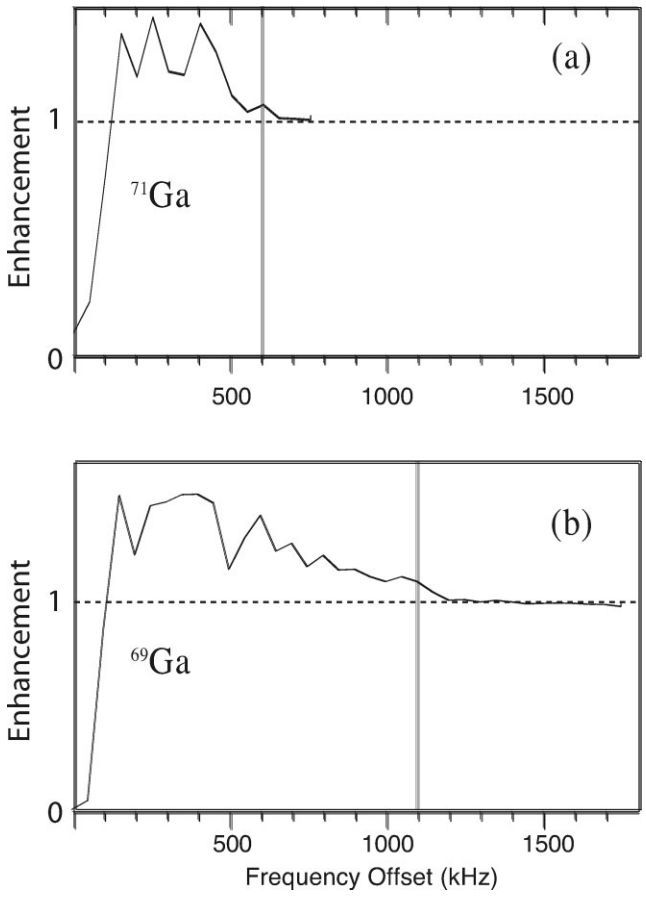

Figure 5. Gallium NMR RAPT of $LaGaO_3$ for both ^{71}Ga (a) and ^{69}Ga (b). The ν_{edge} for each is identified with the vertical line and corresponds to $C_q/2$ for both nuclei.

DISCUSSION

Although there appears to be no clear correlation between η and structure, there is a pronounced decrease in the magnitude of the EFG observed in the pure oxide phases upon modification. In these pure oxide phases, the crystal structure is strained in order to satisfy coordination and stoichiometry. Such strain is manifested by multiple polyhedra sharing the same corner, as well as polyhedra sharing edges and faces. This strain causes a large amount of distortion of the tetrahedra and octahedra. As can be seen in Table 1, the deviation of the bond lengths and bond angles for the pure oxides are, in general, larger than the corresponding deviation in the other structures. This distortion from ideal geometry results in a larger C_q, as the EFG vanishes for perfect tetrahedral and octahedral symmetry. It appears that the conversion of GaO_6 and GaO_4 to GaO_6^{3-} and GaO_4^{-} relaxes the strain as the system shifts so that the oxygen atoms are corner-shared by only two polyhedra. As a result, the magnitude of the EFG drops dramatically, actually becoming very small for one of the sites in gallium sulfate. Also noticeable is the subtle decrease in the magnitude of the EFG of the alkali gallates with the identity of the cation, which is likely attributable to the decrease in charge to volume ratio of the counterion.

Seen in Fig. 7 is a plot of the correlation of eq_{zz} (which is, of course, proportional to C_q) to the chemical shift for the various structural units studied here. There is a clear separation of chemical shift based on coordination number. It appears that the conversion from GaO_6 to GaO_6^{3-} has little effect on the chemical shift, with the same being true of the conversion of GaO_4 and GaO_4^{-}.

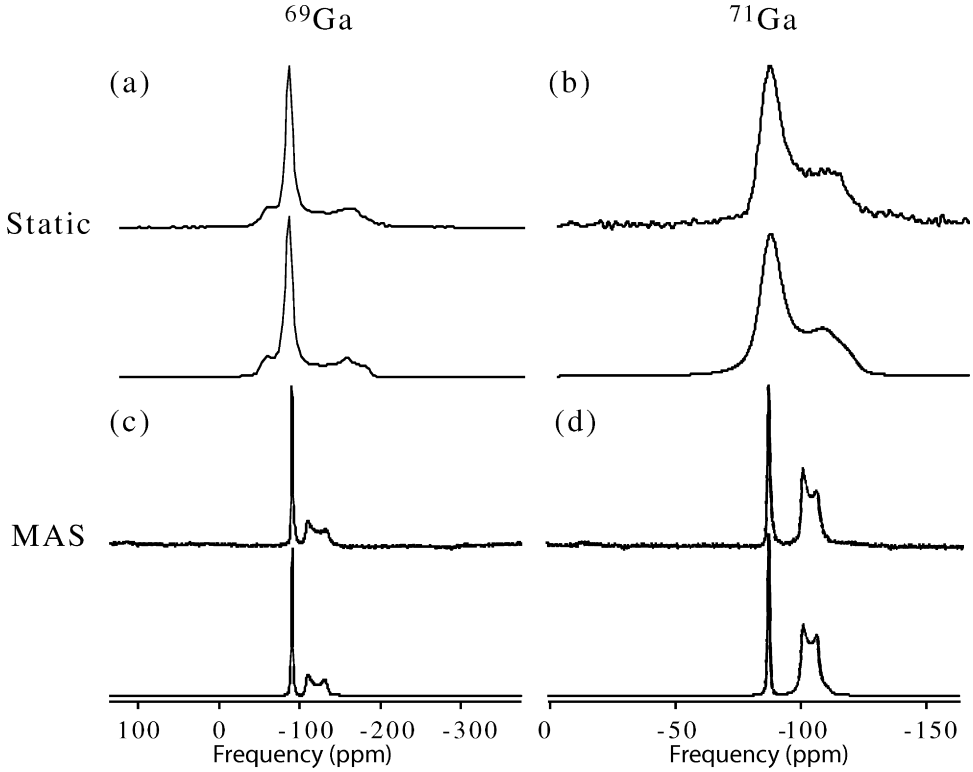

Figure 6. Gallium NMR spectra of gallium sulfate. In (a–d), the experimental spectrum is located on top, with the simulation below. In (a–d) are the ^{69}Ga static, ^{71}Ga static, ^{69}Ga MAS, and ^{71}Ga MAS spectra of $Ga_2(SO_4)_3$, respectively.

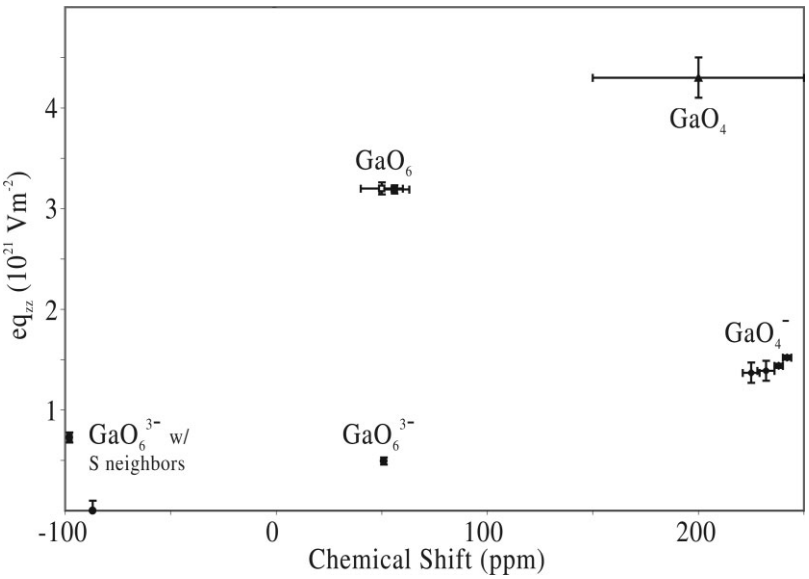

Figure 7. Correlation of the largest component of the EFG tensor to the isotropic chemical shift for various structural units.

Also noteworthy here is the apparent dependence of the chemical shift on the second coordination sphere. Similar results have been observed by Massiot and coworkers in other gallium systems.[33] For virtually all the systems studied here, the oxygen atoms of the gallium polyhedra have been coordinated to other gallium atoms. However, as mentioned previously, the oxygen atoms in the gallium sulfate octahedra are coordinated to sulfur atoms. This shift is apparently not attributable to the polyhedra type, as the other six-coordinate gallium species are coordinated by a variety of polyhedra, yet have virtually indistinguishable chemical shifts.

A final note on chemical shift is the rather small dependence of the gallium chemical shift on the identity of the cation for the alkali metal gallates, despite the fact that the cations are also coordinated to the oxygen atoms. By and large, the cations seem to simply occupy the spaces between the polyhedra and serve to balance the electrostatic charges. Thus, the identity of the cation has little effect on the electron density and, consequently, a small dependence on the chemical shift is observed. However, the gallium and the sulfur atoms are covalently bound, with the oxygen atom serving as the bridge between polyhedra. In such a case, the identity of the bridging ligand can significantly alter electron density.

The previous results suggest that the chemical shift may be helpful in identifying the coordination number of gallium, but that it is not able to distinguish GaO_4 from GaO_4^- and GaO_6 from GaO_6^{3-} However, Fig. 7 shows that these units can be easily differentiated by consideration of the magnitude of the EFG (C_q). The distortions in GaO_4 and GaO_6 are far greater, leading to considerably larger EFGs. The combination of both chemical shift and EFG can be used to assign all the resonances discussed here. Such assignment would be difficult in solution, where the tumbling motion averages the EFG to zero. This suggests that studying gallium oxyanions with solid-state NMR may be more discriminating than doing so in isotropic solution.

CONCLUSION

In the model systems examined here, the magnitude of C_q around gallium was found to vary from zero for one of the GaO_6^{3-} sites in $Ga_2(SO_4)_3$ to 17.4 MHz for the GaO_4 site in β-Ga_2O_3. At larger values of C_q, it becomes difficult to excite the entire Ga solid-state NMR spectrum uniformly, but, as shown here, such problems can be overcome with techniques such as VOCS. For sites with C_q values so small that a second-order lineshape analysis of the central transition is not possible, approaches such as measuring the RAPT enhancement profile, or ST spectroscopy can be used. As expected, the magnitude of C_q is highest in the highly strained octahedral and tetrahedral sites of pure gallium oxides. These strains are relieved in the alkali metal oxides, with the conversion of GaO_4 to GaO_4^- and GaO_6 to GaO_6^{3-}, i.e. as the coordination number of oxygen is lowered to two and the polyhedra shift to strictly sharing corners. A corresponding decrease in the magnitude of C_q is thus observed, as the local octahedral or tetrahedral symmetries become more ideal. The combination of chemical shift and EFG can be used to distinguish among the polyhedra type that cannot be distinguished by chemical shift alone. Such correlations will be helpful for future investigations of more complex systems with gallium NMR.

Acknowledgements

This material is based upon work supported by the National Science Foundation under Grants CHE 0111109. Any opinions, findings and conclusions or recommendations expressed in this material are those of the author(s) and do not necessarily reflect the views of the National Science Foundation.

REFERENCES

1. Ishihara T, Matsuda H, Takita Y. *J. Am. Chem. Soc.* 1994; **116**: 3801.
2. Kröll S, Jusinski LE, Kachru R. *Opt. Lett.* 1991; **16**: 517.
3. Venuto P. *Microporous Mater.* 1994; **2**(5): 297.
4. Bu XH, Feng PY, Stucky GD. *Science* 1997; **278**(5346): 2080.
5. Apseloff G. *Am. J. Ther.* 1999; **6**(6): 327.

6. Einhorn LH, Roth BJ, Ansari R, Dreicer R, Gonin R, Loehrer PJ. *J. Clin. Oncol.* 1994; **12**(11): 2271.
7. Seidman AD, Scher HI, Heinemann MH, Bajorin DF, Sternberg CN, Dershaw DD, Silverberg M, Bosl GJ. *Cancer* 1991; **68**: 2561.
8. Massiot D, Farnan I, Gautier N, Trumeau D, Trokiner A, Coutures JP. *Solid State Nucl. Magn. Reson.* 1995; **4**: 241.
9. Jakobsen HJ, Skibsted J, Bildsøe H, Nielsen NC. *J. Magn. Reson.* 1989; **85**: 173.
10. Yao Z, Kwak H, Sakellariou D, Emsley L, Grandinetti P. *Chem. Phys. Lett.* 2000; **85**: 85.
11. Prasad S, Kwak H, Clark T, Grandinetti PJ. *J. Am. Chem. Soc.* 2002; **124**(18): 4964.
12. Kwak H, Prasad S, Clark T, Grandinetti PJ. *J. Magn. Reson.* 2003; **160**: 107.
13. Frydman L, Harwood JS. *J. Am. Chem. Soc.* 1995; **117**: 5367.
14. Medek A, Harwood JS, Frydman L. *J. Am. Chem. Soc.* 1995; **117**: 12 779.
15. Massiot D, Touzo B, Trumeau D, Coutures JP, Virlet J, Florian P, Grandinetti PJ. *Solid State Nucl. Magn. Reson.* 1996; **6**: 73.
16. Massiot D, Farnan I, Gautier N, Trumeau D, Florian P, Grandinetti P. *J. Chem. Phys.* 1995; **92**: 1847.
17. Massiot D, Montouillout V, Fayon F, Florian P, Bessada C. *Chem. Phys. Lett.* 1997; **272**: 295.
18. Foster LM, Stumpf HC. *J. Am. Chem. Soc.* 1951; **73**: 1590.
19. Remeika J, Marezio M. *Appl. Phys. Lett.* 1966; **8**(4): 87.
20. Slater PR, Irvine J, Ishihara T, Takita Y. *Solid State Ionics* 1998; **107**: 319.
21. Geller S. *J. Chem. Phys.* 1998; **24**: 1236.
22. Grandinetti PJ, Baltisberger JH, Llor A, Lee YK, Werner U, Eastman MA, Pines A. *J. Magn. Reson., Ser A* 1993; **103**: 72.
23. Grandinetti PJ. RMN: a program for one- and two-dimensional NMR data processing. http://www.chemistry.ohio-state.edu/~grandinetti/RMN.
24. Shore J, Vollmer B, Meng Z. *NMR Utilities Software*. South Dakota State University.
25. Sternheimer RM. *Phys. Rev. A. At. Mol. Opt. Phys.* 1972; **5**(6): 1702.
26. Marezio M, Remeika J. *J. Chem. Phys.* 1967; **46**(5): 1862.
27. Geller S. *J. Chem. Phys.* 1960; **33**(3): 676.
28. Åhman J, Svensson G, Albertson J. *Acta Crystallogr. Sect. C. Cryst. Struct. Commun.* 1996; **C52**: 1336.
29. Marezio M. *Acta Crystallogr.* 1965; **18**: 481.
30. Müller H, Hoppe R. *Z. Anorg. Allg. Chem.* 1992; **611**: 73.
31. Krause M, Gruehn R. *Z. Kristallogr.* 1995; **210**: 427.
32. Bastow T, Mathews T, Sellar J. *Solid State Ionics* 2004; **175**: 129.
33. Massiot D, Vosegaard T, Magneron N, Trumeau D, Montouillout V, Berthet P, Loiseau T, Bujoli B. *Solid State Nucl. Magn. Reson.* 1999; **15**: 159.